ORIGINAL ARTICLE

Effect of impact velocity and ligament mechanical properties on lumbar spine injuries in posterior-anterior impact loading conditions: a finite element study

Manon Sterba [1,2,3,4,5] · Carl-Éric Aubin [1,3,4] · Eric Wagnac [4,6,7] · Leo Fradet [1,3,4] · Pierre-Jean Arnoux [2,5]

Abstract

Traumatic events may lead to lumbar spine injuries ranging from low severity bony fracture to complex fracture dislocation. Injury pathomechanisms as well as the influence of loading rate and ligament mechanical properties were not yet fully elucidated. The objective was to quantify the influence of impact velocity and ligament properties variability on the lumbar spine response in traumatic flexion-shear conditions. An L1-L3 finite element spinal segment was submitted to a posterior-anterior impact at three velocities (2.7, 5, or 10 m/s) and for 27 sets of ligament properties. Spinal injury pathomechanism varied according to the impact velocities: initial osseous compression in the anterior column for low and medium velocities versus distraction in the posterior column for high velocity. Impact at 2.7 and 5 m/s lead to higher extent of bony injury, i.e., volume of ruptured bone, compared to the impact at 10 m/s (1140, 1094, and 718 mm^3 respectively), lower L2 anterior displacement (2.09, 5.36, and 7.72 mm respectively), and lower facet fracture occurrence. Ligament properties had no effect on bony injury initiation but influenced the presence of facet fracture. These results improve the understanding of lumbar injury pathomechanisms and provide additional knowledge of lumbar injury load thresholds that could be used for injury prevention.

1 Introduction

Thoracic and lumbar injuries account for 79% of total spinal injuries and usually result from high-energy trauma, particularly high-energy fall (39%) and traffic (26.5%) or sports accidents (5.2%) [1]. The thoracolumbar (TL) region (T10-L2) is the most affected with T12, L1, and L2 being the most frequently injured vertebrae (14.1%, 28.5%, and 12.1% respectively) [1]. Approximately 50% of injuries ranging from low severity bony fractures to complex fracture dislocation may lead to disability [2].

Injury classifications aim to help clinical management and can be based on injury anatomical location [3], suspected injury mechanism (AO classification [4]), or injury morphology

✉ Carl-Éric Aubin
carl-eric.aubin@polymtl.ca

1 Department of Mechanical Engineering, Polytechnique Montréal, Downtown Station, P.O. Box 6079, Montreal, QC H3C 3A7, Canada

2 Laboratoire de Biomécanique Appliquée, IFSTTAR, LBA UMR T24, Aix-Marseille Université, Boulevard Pierre Dramard, Marseille Cedex, France

3 Research Center, Sainte-Justine University Hospital Center, 3175, Cote Sainte-Catherine Road, Montreal, QC H3T 1C5, Canada

4 iLab-Spine (International Laboratory - Spine Imaging and Biomechanics), Montreal, QC, Canada

5 iLab-Spine (International Laboratory - Spine Imaging and Biomechanics), Marseille, France

6 Mechanical Engineering Department, École de technologie supérieure, Montreal, QC H3C 1K3, Canada

7 Research Center, Hôpital du Sacré-Cœur, Montreal, QC H4J 1C5, Canada

("Thoracolumbar Injury Classification and Severity Score" (TLICS) [5]). The AO classification [4] proposed three types of injuries based on the injury mechanism: compression (type A), anterior and posterior element injuries with distraction (type B), and anterior and posterior element with rotation (type C). Type B injuries, known as flexion-subluxation injuries, always involve the posterior ligamentous complex, and may involve the anterior column (vertebral body) leading to minor or extensive instability [6]. Joaquim et al. (2018) classified type B injuries with vertebral translation and facet dislocation as unstable injuries and recommended surgical treatment for these cases [7]. In a clinical context, appropriate treatment strategies are determined from imaging modalities that enable the description of pattern and injury location as well as injury features (e.g., vertebral height loss and vertebral translation) [8]. A better understanding of the link between injury mechanisms, injury morphology, and features may be valuable to help injury prevention and clinical management.

Experimental and numerical studies have been used to identify spinal tolerance, i.e., the levels of force or acceleration that the spine can sustain without major damages [9], and the spine pathomechanisms in traumatic conditions. Most of the published work focused on axial loading because of its importance in the thoracolumbar spine. Axial loading, combined with a preceding flexion, was shown to lead to flexion-subluxation disruption [10]. Recent experimental studies [11] showed that a fall from height can also result in flexion-subluxation injuries. The proposed mechanism was that the initial compressive fracture of the vertebral body subsequently lead to a hyperflexion of the posterior spine. Flexion subluxation may also result from complex loading of the spine due to gross motion or acceleration of the upper body during impact [12]. Fradet et al. (2014) [13] used a comprehensive finite element model (FEM) of the spine to reproduce different types and subtypes of the AO classification by combining forces and moments with different velocities. A combination of sagittal rotation with distractive or compressive force was able to generate flexion-subluxation injuries. Osvalder et al. (1993) [14] experimentally reproduced type B injuries using a cadaveric human functional spinal unit (FSU) by transferring load pulses using a padded pendulum representative of a frontal car crash. They demonstrated that the bending moment at failure increased with the impact velocity but the description of the pathomechanism and final injury pattern was limited to a gross examination of the segment. These studies showed that several loading conditions may lead to flexion-subluxation injuries. However, the pathomechanisms of these injuries as well as the link between their mechanisms (initiation and propagation) and final injury features (extent of bony and soft tissue injuries and vertebral translation) are not yet understood. A better characterization of lumbar injury pathomechanisms and final injury pattern may help to determine safety load limits for complex loading conditions and

resulting injury pattern and extent. It could also help in designing better safety devices.

The posterior ligamentous complex, composed of the ligamentum flavum (LF), the capsular ligament (CL), the supraspinous (SSL), and interspinous ligament (ISL), has a dominant role in resisting spine flexion [15], along with the disc properties and the bone quality in traumatic conditions. They may influence the lumbar injury risk when the spine was submitted to a combination of flexion and shear as it happened during frontal impact in car crashes. Large variability of ligaments' mechanical properties is depicted in the literature according to strain rate, age, intersubject variability, and different experimental setup [16–18]. This variability was shown to affect the biomechanics of the lumbar spine under physiological daily life loading [18–20] but little work has been done regarding the effect of this variability in traumatic conditions. Moreover, the loading rate should affect spinal injury during a traumatic event [21, 22]. Finite element modeling enables the comparison of the kinetic response for controlled loading rates as well as the study of stress distribution and failure propagation that are difficult to obtain in experimental studies and may be used to improve the understanding of spinal injury pathomechanisms. A better understanding of injury initiation site, kinetic thresholds, and injury propagation is, for instance, necessary to improve safety device designs that are used at various velocities.

The objective was to quantify the influence of impact velocity and posterior ligament properties variability on the mechanical response of the lumbar segment in traumatic flexion-shear condition.

2 Methods

2.1 Finite element model development

A previously validated FEM of the spine, the Spine Model for Safety and Surgery (SM2S) [13, 23, 24], was selected for this study. The geometry was obtained from a CT scan reconstruction of a 50th percentile healthy male volunteer with no recent spinal pathology. The FEM was composed of cortical and cancellous bone modeled by shell and solid elements respectively. The bone behavior was governed by a strain rate-dependent elasto-plastic law (Jonhson-Cook) with a failure model based on the maximal strain. Each element that reaches the failure criteria was deleted from the model to represent the failure propagation [24]. Each vertebra was divided into seven cancellous and nine cortical regions with specific material properties and cortical thickness respectively [24]. The disc was represented by eight-node hexahedral elements separated in two parts representing the annulus fibrosus (AF) and the nucleus pulposus (NP). Each part was governed by a hyperelastic law based on a first-order Mooney-Rivlin

formulation [25]. The collagen fibers were modeled as nonlinear springs for each of the six layers of AF [26]. The zygapophyseal facet joints were modeled with frictionless contact interfaces. The mesh of the isolated L1-L3 FEM contained 52,332 nodes and 238,383 elements, with lengths varying from 0.5 to 2.5 mm. Details of models properties including material properties and mesh size selection were investigated previously [23, 24, 27] and the model was already used to investigate spinal trauma biomechanics [13, 24]. The material properties are summarized in Table 1. The six major ligaments, anterior and posterior longitudinal ligament (ALL and PLL), LF, CL, ISL, and SSL, were represented using geometric data (cross-sectional area and length) taken from a cadaveric study [28]. An anisotropic nonlinear elastic law including the toe region and a failure criteria based on maximal principal strain modeled their behavior in the principal fiber direction. For bone and ligaments, the failure is modeled using an element deletion method once the ultimate deformation level is reached within a given element. The corresponding mechanical parameters implemented in the FEM were the strain at the end of the toe region (ε_{TR}), the Young modulus (E), and the failure strain (ε_{FAIL}) (Table 2). Intertransverse ligaments were not modeled assuming they have a very low biomechanical importance in the lumbar region, particularly in flexion [29].

To assess the effects of ligament properties variability, several stress-strain curves (defined by ε_{TR}, E, and ε_{FAIL}) were generated. To do so, a three-level full factorial design of experiment (DOE) was used to generate 27 stress-strain curves that were successively implemented in the FEM. Please note that "level" refers here to the statistical analysis. For each factor (one of the three law parameters), the high level corresponds to the maximal value that can be assigned to the factor whereas the low level corresponds to the minimal one. Because of their functional and anatomical differences, distinct properties were determined for each ligament (Table 2) as explained here after. The high levels for E, and the low and high ε_{FAIL} were defined according to mechanical tests approximated from cadaveric tensile test on lumbar ligaments, or subaxial cervical ligaments when lumbar dynamic data were unavailable [16, 28, 30, 31], as subaxial cervical and lumbar ligaments have similar anatomy and function [32]. The value for ε_{TR} and low level for E were obtained differently because experimental tensile tests do not appropriately represent the toe region [33] because of dissection and preconditioning. No toe region (i.e., $\varepsilon_{TR} = 0$) was assumed for the low level, whilst the high level of ε_{TR} and low level of E were obtained by calibrating ε_{TR} and E of a lumbar FSU under flexion-extension flexibility test combined with stepwise reduction as proposed by Schmidt et al. (2007) [34]. The resulting range of motion for high ε_{TR} and low E was within the experimentally documented range [35]. The middle levels were determined as the mean of the lower and higher

levels. ε_{TR} and E have a combined effect on the global stiffness of the segment: the stiffest segment had a null ε_{TR} and high E whereas the most flexible one had a high ε_{TR} and low E.

2.2 Study of the failure pattern at L2 and of the global kinetic response

The 27 sets of ligament stress-strain curves were implemented in the L1-L3 FEM which was submitted to traumatic flexion shear that can happen during frontal car collisions. The traumatic flexion shear was approximated with a posterior-anterior impact to the virtual center of mass of the upper body, reproducing existing experimental setup [14]. This lead to a combination of flexion moment and shear and distraction force. The z-axis was pointing downwards, representing the axial direction, and the y-axis was oriented horizontally, aligned with the segment's antero-posterior axis, and directed posteriorly. A horizontal initial velocity was applied to a point located at 300 mm above the L2-L3 FSU mid-disc plane [14]. A mass of 12 kg, as used in experimental study [14], was applied to the center of mass rigidly linked to the upper part of the L1 vertebra. L3 was fixed in all directions. The distance between the gravity line passing through the virtual center of mass of the upper body and the center of L3 was 21 mm [36]. Gravity was applied to the model with a kinetic relaxation method until a steady state was reached before the application of the posterior-anterior impact. The relaxation method consisted of numerically resetting the kinetic energy to zero each time it reached a maximum, to reach a steady state. This was done to apply the gravity over a short period of time without generating numerical instabilities. Three impact velocities were tested: 2.7 m/s (low dynamics), 5 m/s, and 10 m/s (high dynamics) (Fig. 1). This corresponds to an angular velocity of the FSU of 0.2, 0.35, and 1.1°/ms. These values were chosen to be high enough to lead to spinal injury [14]. The final design of experiments, including the impact velocities and the sets of ligament properties, resulted in 81 simulations (27 sets of ligament stress-strain curves tested at each of the three impact velocities).

The 81 simulations were run using the explicit commercial finite element solver Radioss v 14.0 (Altair Engineering Inc., Troy, MI). The resulting pathomechanism was described by using the global kinetic response of the segment as a function of simulation time (maximal bending moment, maximal forces (shear, tensile, and compressive)), and axial stress distribution at the time of failure initiation (time at which a first solid element exceeded its failure criteria). The final pattern of injury was quantitatively defined by the location and the volume of ruptured bone that represents the extent of bony injury (volume of solid elements that exceeded the failure criteria) and the horizontal displacement of L2. The simulations were stopped after the complete disruption of the spine was

Table 1 Mechanical properties of bony tissues and of the disc in the model (adapted from [24])

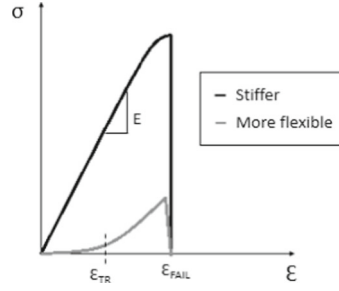| Material properties of bony tissues	Cancellous bone (per zone) and bony endplate center (B) (Cf. figure (b) below)							Cortical bone and bony endplate margin
	A	B	C	D	E	F	G	
Density ($\times 10^{-3}$ g/mm^3)	1.8	1.8	2.0	2.0	2.5	2.5	1.8	0.2
Modulus of elasticity, E (MPa)	93.7							4,014
Poisson's ratio, m	0.25							0.3
Yield stress, a (MPa)	1.95							105
Hardening modulus, b (MPa)	8.5	7.0	8.5	8.1	12.5	12.5	7.0	492.9
Hardening exponent, n	1							1
Failure plastic strain, ep	0.082	0.06	0.082	0.08	0.104	0.104	0.06	0.071
Maximum stress (MPa)	2.65	2.3	2.65	2.6	3.25	3.25	2.3	140
Strain rate coefficient, c	0.533							0.272
Reference strain rate, _e0	0.008							0.008
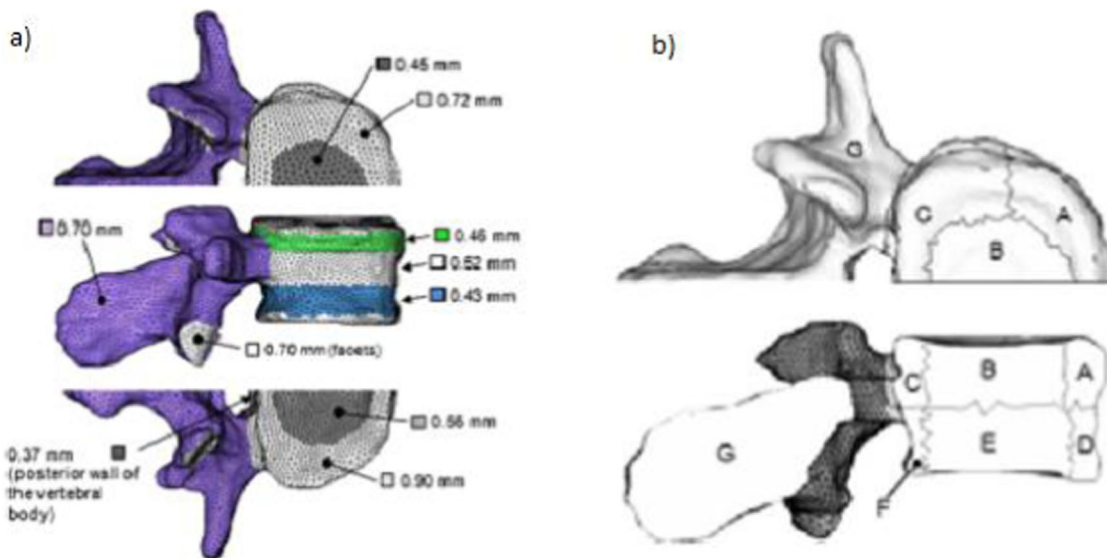
Subdivision of the vertebra into nine zones of different cortical bone thicknesses (a) and seven zones of different material properties (b)

Material properties of the disc	Nucleus pulposus	Annulus matrix	Fibers
Density (E^{-6}kg/mm^3)	1	1.2	–
Poisson's ratio, v	0.499	0.45	–
C10	31.8	11.8	–
C01	-8.0	-2.9	–
Load–disp. Curve	–	–	Nonlinear

achieved. Lastly, the pattern of injury was graphically identified according to the AO classification. In the context of the design of experiments, we used an ANOVA (Statistica, v10 software, Statsoft, Tulsa, OK) to analyze the individual and combined effects of the impact velocities and of the material properties ($p < 0.01$).

Table 2 Ligament properties used for the design of experiments for anterior and posterior longitudinal ligament (ALL and PLL), ligamentum flavum (LF), capsular ligaments (CL), interspinous ligament (ISL), and supraspinous ligament (SSL)

		ALL	PLL	LF	CL	ISL	SSL
ε_{TR}	low level	0	0	0	0	0	0
	middle level	0.005	0.15	0.25	0.25	0.25	0.25
	high level	0.01	0.3	0.5	0.5	0.5	0.5
E (MPa)	low level	40	50	5	5	5	20
	middle level	73	96	17.3	8.4	17.5	34
	high level	106	142	29.5	11.8	29.9	48
ε_{FAIL}	low level	0.4	0.7	0.5	0.7	0.4	0.7
	middle level	0.8	1.0	0.7	0.9	0.5	1.0
	high level	1.2	1.2	0.8	1.1	0.6	1.2

3 Results

3.1 Analysis of impact velocity

Impacts at 10 m/s resulted in higher maximal bending moment, shear, and distractive forces and lower flexion angle at failure initiation compared to 2.7 and 5 m/s ($p < 0.01$). Simulated peak compressive forces generated in high dynamic impacts were lower than for medium and low impacts (495 N, 1797 N, and 1403 N respectively) (Table 3).

For impact velocities of 2.7 m/s and 5 m/s, maximal axial stress in solid element of the cancellous bone was in compression and located anteriorly in the vertebral body (9.7 MPa ± 3.8 and 8.7 MPa ± 1.2 respectively). The failure was slightly delayed after the peak of compression force for the lowest impact velocity (2.7 m/s) and at the peak of compression force for impact velocity of 5 m/s. For impact velocity of 10 m/s, the maximal axial stress in the cancellous bone was in tension, located posteriorly in the vertebral body (9 MPa ± 1.8), and lead to the initiation of the failure. For impact velocity of 10 m/s, the initiation of failure happened at the peak of tensile force (Fig. 2).

Figure 3 describes the load sharing between the posterior ligaments, the articular facets, and the disc at the time of failure initiation for the three impact velocities. Mean axial force exerted by the posterior ligamentous complex and facet contact forces were higher for high impact velocity (1240 N and 170 N respectively) than for the low one

(712 N and 26 N respectively). The maximal intradiscal pressure was positive for low and medium impact velocity, indicating a compression of the intervertebral disc and negative for high impact velocity, indicating a distraction of the intervertebral disc (Fig. 3).

The different impact velocities resulted in different types and subtypes of injuries. Low and medium impact velocities produced inferior or superior wedge fracture with major (defined as B.1.2.1 in the AO classification [4]) or minor posterior ligamentous complex injury (comparable to A.1.2 in the AO classification [4]). High impact velocity induced flexion subluxation with (B.1.1.3) or without anterior dislocation (B.1.1.1) (represented by anterior displacement of L2 and facet failure) (Fig. 4). Complete rupture of the PLC, i.e., complete rupture of the LF, CL, ISL, and SSL, was observed in 3, 8 and 12 simulations for low, medium and high impact velocity. The complete failure happened at the L1-L2 level for low and medium velocity and at L2-L3 level for high velocity. At high impact velocity, ISL and CL of the L2-L3 level was ruptured for all simulations whereas only the ISL was injured in 17 simulations for both low and medium impact velocity.

The anterior displacement of L2 induced at impact of 10 m/s was 3.7 times as much as the one for impact at 2.7 m/s and 1.4 times as much as the one for the impact at 5 m/s ($p < 0.01$). Impact at 10 m/s produced about 37% less volume of ruptured bone than impact at 2.7 m/s ($p < 0.01$) but resulted in higher occurrence of facet fracture with a mean volume of 49 mm^3 in articular facet region (Table 4).
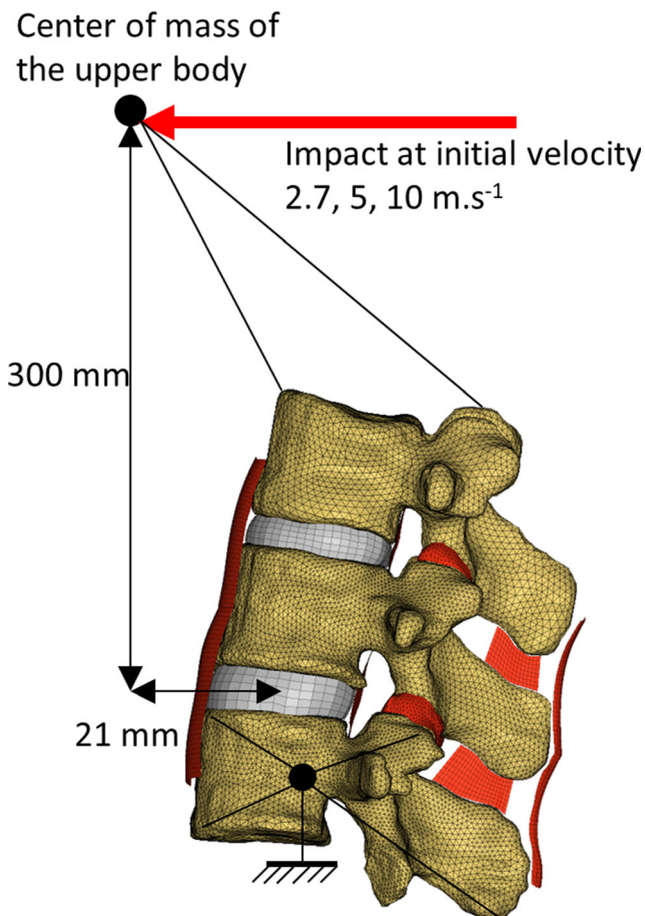
Fig. 1 Finite element simulation of a posterior-anterior impact applied to the virtual center of mass of the upper body

3.2 Effect of the mechanical properties of posterior ligamentous complex

For a given impact velocity, the same pathomechanisms and location of injury initiation (anterior or posterior part) were observed for all of the 27 combinations of ligament properties. The strain at the end of the toe region (ε_{TR}) and Young's modulus (E) had a significant influence on the maximal moment, the maximal axial force (tensile and compressive), and the maximal shear force ($p < 0.01$). The maximal moment and

the maximal shear force were higher for the stiffest models than for the more flexible ones for the three velocities. Compared to the most flexible ones, the stiffest models resulted in higher compressive force at low and medium velocities, and in lower maximal tensile force at high impact velocities. The results are shown in Fig. 5. ε_{TR} and E had a significant influence on the facet contact force at failure and on the volume of ruptured bone localized in articular facet region ($p < 0.01$), which was almost null for the most flexible models and increased with the global stiffness (i.e., higher E and lower ε_{TR}). For the highest impact velocity, the volume of rupture bone at the articular facets increased with increasing E and decreasing ε_{TR}, i.e., it increased with the global stiffness of the segment and lead to anterior dislocation (B.1.1.3 in Fig. 4).

4 Discussion

The effects of impact velocity and ligament properties on the pathomechanisms of the osteoligamentous lumbar spine were tested. A previous study was performed on a two-vertebra model to verify the model against experimental data. The mean maximal moment and shear force for the 27 sets of ligament properties were 158 Nm and 512 N respectively compared to 185 Nm and 600 N for experimental results [14]. The three-vertebra model predicted maximal bending moment of 183 ± 48 Nm which agrees well with experimental measurements for flexion-shear loading on three-vertebra thoracolumbar segments (174 ± 58 Nm [37]).

Different impact velocities resulted in different mechanisms and location of injury initiation. For low and medium impact velocities, the lumbar spine failed in compression in the anterior part of the vertebral body. The initial osseous injury of the anterior column lead to a hyperflexion and failure of the posterior part of the vertebral body and might extend to the posterior ligamentous complex. Ivancic et al. [11] found similar mechanisms when they experimentally reproduced a fall from height. Maximal compressive forces in these conditions were 1.6 ± 0.44 kN and were comparable to experimental observations 1.98 ± 0.27 kN [37]. These values are lower

Table 3 Kinetic and kinematic responses during impact simulations. Mean and standard deviation ($n = 27$) of the model responses for each impact velocity (2.7, 5, and 10 m/s) (*$p < 0.01$)

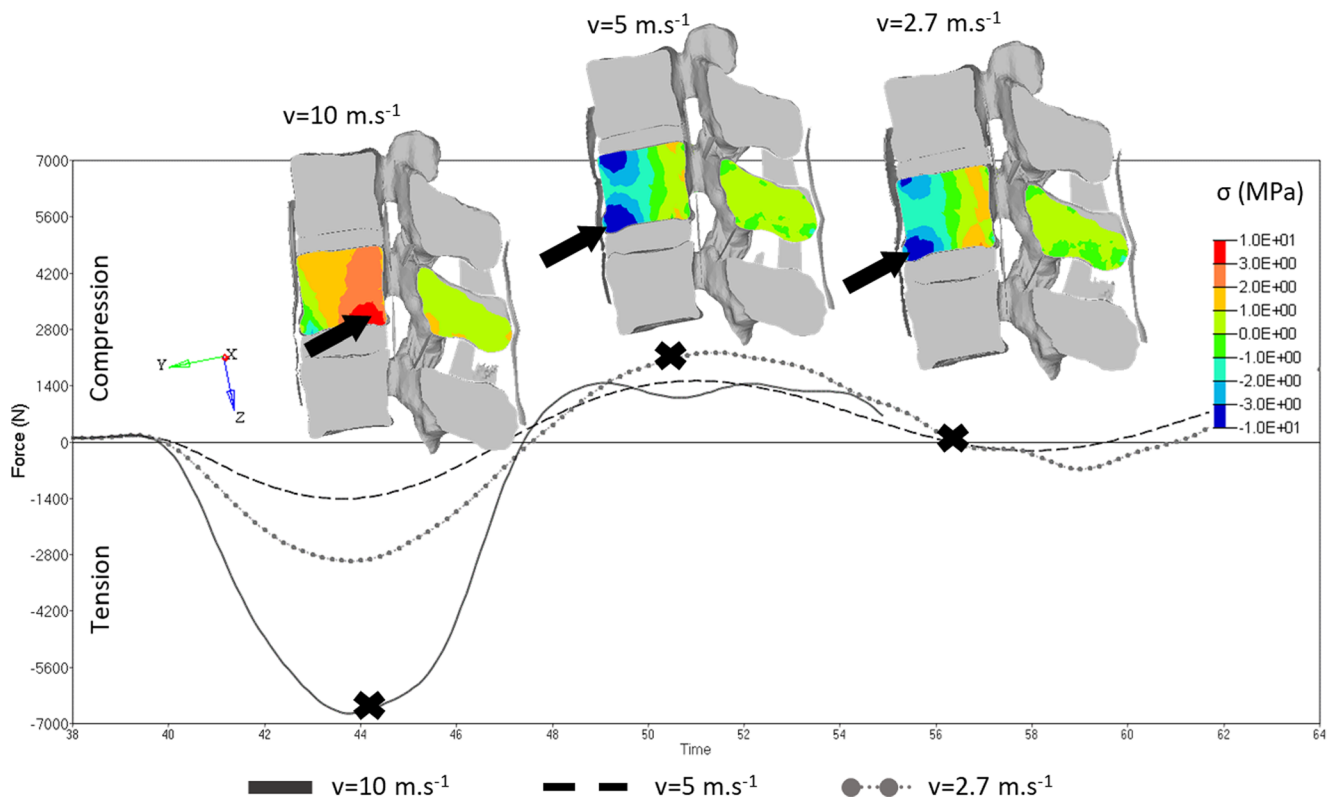|	$V = 2.7$ m/s	$V = 5$ m/s	$V = 10$ m/s
Time at failure initiation (ms after impact)	17 ± 0*	9 ± 2*	3 ± 0*
Flexion angle (°)	7.6 ± 0.2*	7.1 ± 1.7	3.2 ± 0*
Maximal moment (Nm)	139 ± 17*	177 ± 20*	235 ± 41*
Maximal shear force (N)	872 ± 192*	1391 ± 104*	2092 ± 151*
Maximal tensile force on L2 vertebral body (N)	1506 ± 45*	3158 ± 98*	7234 ± 202*
Maximal compressive force on L2 vertebral body (N)	1403 ± 346*	1797 ± 430*	495 ± 438*

Fig. 2 Evolution of the axial force during the impact simulation for each impact velocity for the stiffest ligament properties. For each impact velocity, the stress distribution (axial stresses were positive in tension and negative in compression) within L2 is shown at the time of bony failure initiation (time is indicated on corresponding curve by a cross). Solid arrows point the location of the first deleted element (failure initiation)

than compressive failure force in compression-only mechanisms (4.9–14.9 kN) [38]. This confirms that the spinal injury tolerance changes with the loading environment [21] and highlights the need for spinal tolerance characterization for specific loading conditions. In the case of a high impact velocity (10 m/s), distraction of the posterior element caused an initial ligamentous and osseous injury that propagated to the anterior column. The different impact velocities resulted in different combinations of pure loads in terms of magnitude and direction and thus influenced the load sharing in the

lumbar spine. Low and medium impact produced higher compressive force and lower moment. In these conditions, the disc and the vertebral body supported higher loads than the posterior elements. The resultant injuries were associated with a higher volume of ruptured bone in the vertebral body and resulted in a higher anterior height reduction compared to injury resulting from high impact. At 10 m/s, higher moment and shear force were observed and explained the increase in ligament and facet contact forces. These injuries were characterized by a major or complete rupture of the PLC, a higher
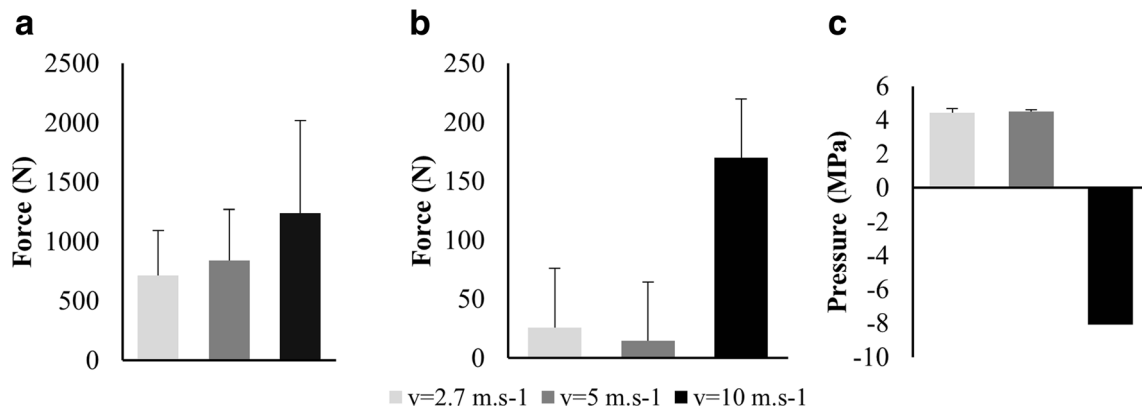

Fig. 3 Mean axial force exerted by the ligaments on L3 posterior elements (A), L2-L3 facet contact force (B), and L2-L3 intradiscal pressure at failure initiation (C)
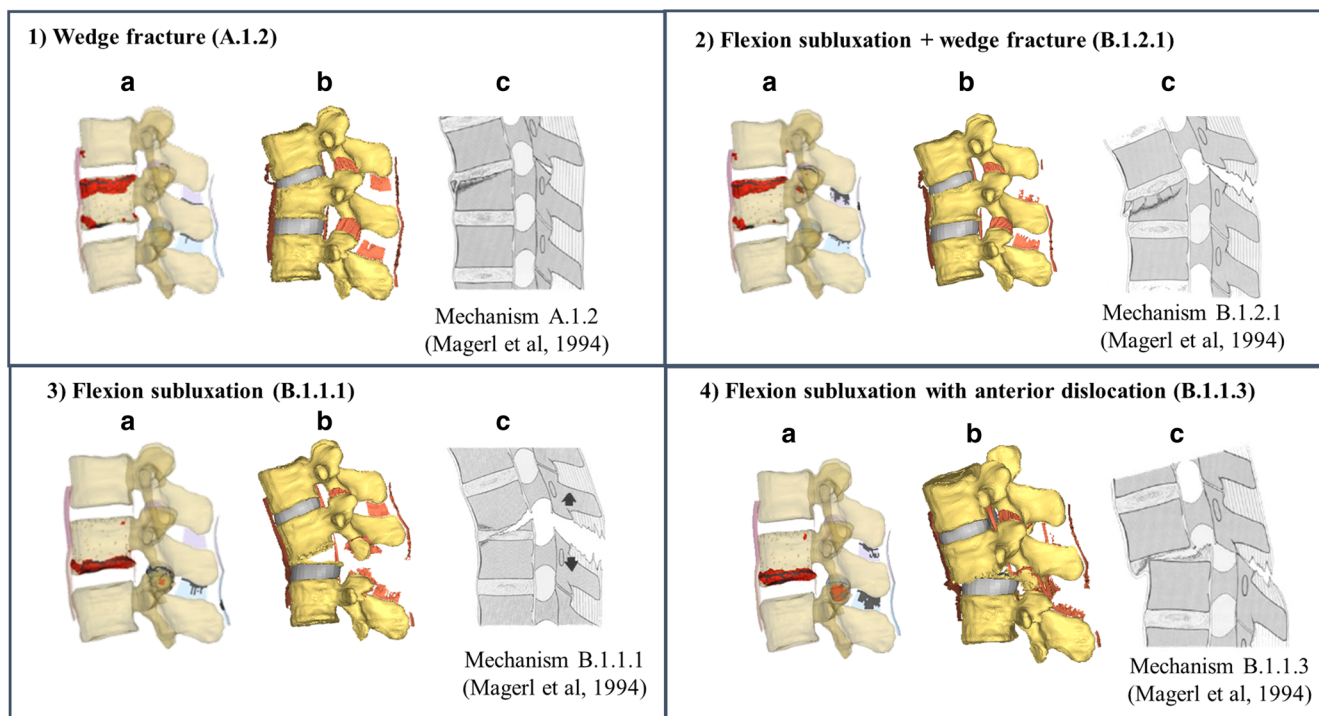
Fig. 4 Graphic representation of the four injury patterns observed for the simulated posterior-anterior impact conditions: (1) wedge fracture and (2) flexion subluxation and wedge fracture due to posterior-anterior impact at 2.7 or 5 m/s; (3) flexion subluxation and (4) flexion subluxation with anterior dislocation due to posterior-anterior impact at 10 m/s. (A) shows the ruptured cancellous bone elements in red and ligaments in gray using the initial model; (B) shows a representation of the resultant deformed model with the failed cancellous bone and ligaments; (C) corresponding failure mechanism of the AO classification (Magerl et al. 1994) [4]

anterior displacement, and a higher occurrence of facet failure. The horizontal displacement of one vertebra of the segment increased the risk of impairment of the spinal cord because of the reduction of the sagittal diameter of the foramen vertebral [39]. These injuries may represent a higher risk of neurological deficit. The injury severity (type of injury, facet failure occurrence, vertebral translation) increased with the impact velocity, i.e., with the accident severity, which agreed with other findings [40]. Obviously, the tested scenarios of this study do not represent all possible accident mechanisms, which may have a combination of loads and directions of impact [41]; however, the developed model could be used to further test more complex conditions, or the results could be used to infer intermediate situations. Ligament properties had

no effect on the injury initiation (mechanisms and location). The kinetic responses were mainly influenced by the impact loading conditions, but two of the tested properties (E and ε_{TR}) also influenced the resultant forces and moments by modifying the internal loads. Therefore, higher resultant bending moments and shear forces were measured for the stiffest models than for the more flexible ones for the three impact velocities. For the low and medium impact velocities, an increase in stiffness was associated with an increase of compressive force, intradiscal pressure, and facet contact force because of the higher resistance of the PLC that may impact the segment motion. As expected, for high impact velocity, the tensile force measured at the L3 vertebral body was lower for the stiffest models than for the more flexible because of the higher

Table 4 Injury characteristics for the 27 simulations for each of the three tested impact velocities. Mean and standard deviation ($n = 27$) for each impact velocity (2.7, 5, and 10 m/s) (*$p < 0.01$)

|	$V = 2.7$ m/s	$V = 5$ m/s	$V = 10$ m/s
Volume of ruptured bone (mm³)	1140 ± 506*	1094 ± 182*	718 ± 338*
Number of simulated cases with facet failure (of the 27 simulations)	2	7	16
Volume of ruptured bone at facet joint (mm³)	4 ± 17*	10 ± 43*	49 ± 103*
Horizontal displacement of L2 with respect to L3 (mm)	2.1 ± 0.1*	5.4 ± 0.1*	7.7 ± 1.4*
Types and number of simulated scenarios of injury according to the AO classification (Magerl et al. 1994) [4]	A.1.2 (17) B.1.2.1 (10)	A.1.2 (17) B.1.2.1 (10)	B.1.1.1 (22) B.1.1.3 (5)
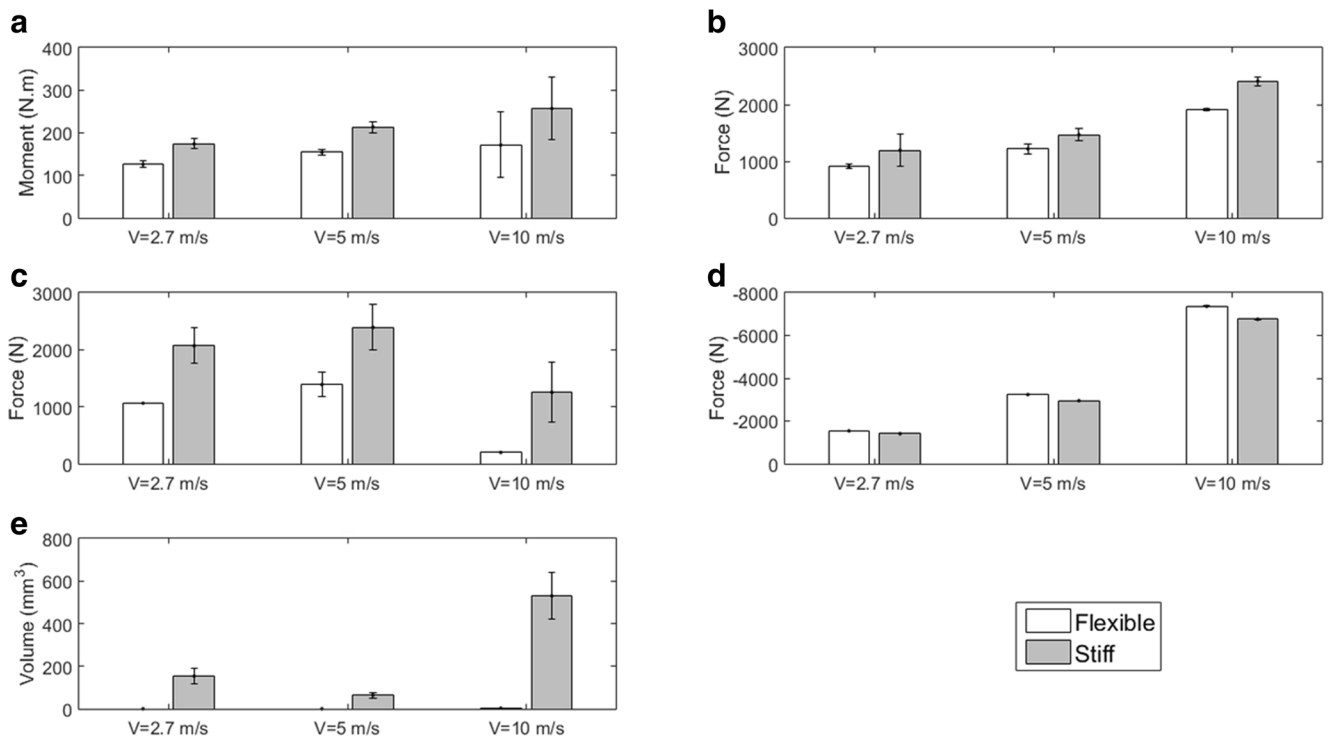
Fig. 5 Bar plot comparing the mean (±SD) (for three values of failure strain) kinetic response between the stiffest models (gray bars) and the most flexible ones (white bars) for each of the three tested impact velocities: mean maximal moment (A), shear force (B), compressive force (C), and tensile force (D) on vertebral body and volume of ruptured bone at facet joint (E)

resistance of the PLC in the first case. The global stiffness influenced the final injury pattern, particularly the presence of facet failure. At high impact velocity, stiffer models (high E and/or low ε_{TR}) were associated with higher occurrence of facet failure and lead to fracture dislocation, i.e., the articular processes had slid past each other. This may result in higher degree of instability compared to flexion subluxation without permanent facet damage. We may hypothesize that stiffer ligaments resulted in more constrained motion at the articular facet, thus leading to higher stresses in this area.

This numerical simulation study presents some limitations. We chose a large range of variability by using available data for lumbar ligaments under quasi-static loading conditions and cervical ligaments under high dynamic loading. This enables us, in a comparative manner, to assess the potential effect of spine flexibility. Better range may be chosen when experimental data will be available. In this study, the effects of the impact velocity and ligament properties were tested as independent factors, in part because of the lack of available data. Moreover, the viscoelastic formulation did not represent the initial toe region of the ligaments, which is important to model spinal motions. Then, the ligament behavior was simplified as being not strain rate dependant. In future studies, a viscoelastic representation, which includes the toe region, would be useful to further test traumatic conditions. Only variations of ligament properties were studied considering properties of bone and intervertebral discs as fixed. The bone

properties used were previously verified and used to assess spinal injury mechanisms [13]. The disc behavior was modeled by a hyperelastic material law. Despite more complex poro- and/or viscoelastic models being valuable to describe the long-term behavior of the disc, in impact loading, the increasing stiffness as represented by a hyperelastic law enables to have a first-order representation of the disc behavior and the segment risk of failure [42]. The disc material properties were fixed at previously identified dynamic properties [26]. Indeed, it is expected that the disc properties are rate-dependent. However, even if a great difference in the disc behavior was found between quasi-static and dynamic conditions [26], the dynamic properties used in this study are thought to be valid for a range of traumatic loading conditions for the context of the current study. The calibration and verification process of the disc was limited to axial compression [26]. However, these properties were used in an entire lumbar spine model verified against experimental data obtained for dynamic flexion and extension [24]. In this study, we focused on the osseo-ligamentous mechanisms of failure and did not include a model of the disc failure, which prevents to comprehensively analyze the disc injuries. However, we may assume that the forces and injuries that happened at the endplates of the vertebral bodies will propagate in the disc. A more complete study of the ossseo-disco-ligamentous failure was beyond the scope of the current study, but could be the subject of a future study, which would require the development of a

disc model of failure. The simulation results for the highest velocity were interpreted as B 1.1 injuries of the AO classification as the osseo-ligamentous flexion-subluxation subcomponents were coherent with simulations. In this comparative study, an available detailed experimental model was reproduced in order to define repeatable accident-like conditions that induced flexion, shear, and compression in the lumbar spine. Other mechanisms (such as extension, rotation, and lateral bending) were not included in this study because of the lower influence of the ligaments in these failure mechanisms. The selected loading conditions were intended to represent a possible frontal impact [14] but the resultant spine loading may represent other accident types such as fall from height which can also lead to concomitant failure of posterior elements and vertebral bodies [11]. The different velocities chosen in this study allow to represent different accident and injury severities. The lowest impact velocity selected corresponds to a sufficient velocity at which the upper body region would be displaced due to a collision [14], and does not represent the velocity of a vehicle at the time of impact. The highest velocity tested corresponds to an impact at 36 km/h, which is obviously not the highest speed for an accident. A higher impact velocity could be tested in a future study to verify if the mechanism of failure would differ for higher impact velocity. The stress distribution and failure pattern was studied at L2, which was away from the boundary conditions imposed on the model (i.e., L3 was considered as a rigid body fixed in all directions and the impact was applied to a node rigidly linked to L1 to model the displacement of the upper body weight). The global posture of the subject (location of the center of mass of the upper body and lumbar lordosis) was also fixed. The location of the center of mass was chosen according to literature data [14, 36]. Under compression, the impact velocity was shown to be the first factor influencing the lumbar injuries followed by the posture [22], suggesting that the comparative results of this study are valid for several postures. A weight of 12 kg was used to reproduce the experimental setup [14]. This weight was lower than expected for an average adult but it was chosen to avoid instability during preloading considering the absence in the model of muscles to stabilize the spine. A higher weight was tested (40 kg) and similar failure mechanisms and patterns were found for each impact velocity. A lower weight was deemed appropriate for a comparative study. These boundary conditions were not meant to be fully physiological, but to standardize the way to comparatively describe the failure characteristics at L2, for different impact severities and different ligament properties. Articular cartilage was not modeled and this may influence the facet joint biomechanics. However, we think that the relative results that we found between different impact velocities and different ligament properties will still be valid in the presence of cartilage. No muscles were implemented in the FEM but the role of muscles in traumatic events is limited due to their delayed activation [43].

To date, axial compressive force is the primary lumbar spine injury metrics used as injury criteria. However, this metric does not account for the variation in loading environment and in lumbar spine geometry/material properties [12]. Our results show that a compression failure of the anterior column may happen below the compressive failure force when it is caused by a combination of flexion and shear and can lead to failure of the posterior ligamentous complex. This suggests a need for more study on the lumbar injury tolerance under complex loading to developed robust injury criteria. Next steps will be to compare lumbar injury threshold and pathomechanisms under different complex loadings for different bone and intervertebral disc material properties and spinal geometry.

5 Conclusion

The FEM used in this study enabled a detailed characterization of the lumbar injury under traumatic conditions. The impact velocity modified the injury pathomechanism and final injury pattern. This was shown in the case of a posterior-anterior impact causing a combination of flexion, shear, and distraction in the lumbar spine. For low and medium impact velocities, initial osseous injury happened under compression forces in the anterior column whereas high dynamic impact caused pure distraction injury with very low compressive stresses in the segment. Less volume of ruptured bone was found for a high impact velocity. However, we found more anterior displacement and higher occurrence of facet fracture, suggesting a higher risk of neurological deficit and long-term instability. Stiffest segments were associated with a higher risk of permanent facet damage. A detailed characterization of the lumbar pathomechanisms is crucial for the establishment of more robust lumbar injury criteria for injury prevention. These results and further use of the FEM may also provide valuable information to deduce impact severity from injury pattern.

Publisher's note Springer Nature remains neutral with regard to jurisdictional claims in published maps and institutional affiliations.

References

1. Leucht P, Fischer K, Muhr G, Mueller EJ (2009) Epidemiology of traumatic spine fractures. Injury 40:166–172

2. Rajasekaran S, Kanna RM, Shetty AP (2015) Management of thoracolumbar spine trauma: an overview. Indian J Orthop 49:72–82

3. Denis F (1983) The three column spine and its significance in the classification of acute thoracolumbar spinal injuries. Spine 8:817–831

4. Magerl F, Aebi M, Gertzbein SD, Harms J, Nazarian S (1994) A comprehensive classification of thoracic and lumbar injuries. Eur Spine J 3:184–201

5. Vaccaro AR, Lehman RA Jr, Hurlbert J, Anderson PA, Harris M, Fehlings MG et al (2005) A new classification of thoracolumbar injuries. Spine 30:2325–2333

6. Aebi M (2010) Classification of thoracolumbar fractures and dislocations. Eur Spine J 19:2–7

7. Joaquim AF, Patel AA, Schroeder GD, Vaccaro AR (2018) A simplified treatment algorithm for treating thoracic and lumbar spine trauma. J Spinal Cord Med:1–11

8. Santiago FR, Muñoz PT, Sánchez EM, Paniza MR, Martínez AM, Abela ALP (2016) Classifying thoracolumbar fractures: role of quantitative imaging. Quant Imaging Med Surg 6:772–784

9. Yoganandan N, Nahum AM, Melvin JW (2014) Accidental injury: biomechanics and prevention. Springer, Berlin

10. Hoshikawa T, Tanaka Y, Kokubun S, Lu WW, Luk KD, Leong JC (2002) Flexion–distraction injuries in the thoracolumbar spine: an in vitro study of the relation between flexion angle and the motion axis of fracture. Clinical Spine Surgery 15:139–143

11. Ivancic PC (2014) Biomechanics of thoracolumbar burst and chance-type fractures during fall from height. Global Spine J 4:161–168

12. Stemper BD, Pintar FA, Baisden JL (2015) Lumbar spine Injury biomechanics. In: Yoganandan N, Nahum AM, Melvin JW (eds) Accidental injury: biomechanics and prevention. Springer, New York, pp 451–470

13. Fradet L, Petit Y, Wagnac E, Aubin CE, Arnoux PJ (2014) Biomechanics of thoracolumbar junction vertebral fractures from various kinematic conditions. Med Biol Eng Comput 52:87–94

14. Osvalder AL, Neumann P, Lövsund P, Nordwall A (1993) A method for studying the biomechanical load response of the (in vitro) lumbar spine under dynamic flexion-shear loads. J Biomech 26:1227–1236

15. Lee KK, Teo EC (2005) Material sensitivity study on lumbar motion segment (L2-L3) under sagittal plane loadings using probabilistic method. J Spinal Disord Tech 18:163–170

16. Mattucci SF, Moulton JA, Chandrashekar N, Cronin DS (2012) Strain rate dependent properties of younger human cervical spine ligaments. J Mech Behav Biomed Mater 10:216–226

17. Clarke EC, Appleyard RC, Bilston LE (2007) Immature sheep spines are more flexible than mature spines: an in vitro biomechanical study. Spine 32:2970–2979

18. Coombs DJ, Rullkoetter PJ, Laz PJ (2016) Quantifying variability in lumbar L4-L5 soft tissue properties for use in finite-element analysis. J Verif Valid Uncert 1:031007

19. Naserkhaki S, Arjmand N, Shirazi-Adl A, Farahmand F, El-Rich M (2018) Effects of eight different ligament property datasets on biomechanics of a lumbar L4-L5 finite element model. J Biomech 70:33–42

20. Putzer M, Auer S, Malpica W, Suess F, Dendorfer S (2016) A numerical study to determine the effect of ligament stiffness on kinematics of the lumbar spine during flexion. BMC Musculoskelet Disord 17:95

21. Schmitt K-U, Zürich PFNE, Muser MH, Walz F (2013) Trauma biomechanics: introduction to accidental injury. Springer Science & Business Media, Berlin

22. Zheng J, Tang L, Hu J (2018) A numerical investigation of risk factors affecting lumbar spine injuries using a detailed lumbar model. Appl Bionics Biomech 2018:1–8

23. El-Rich M, Arnoux P-J, Wagnac E, Brunet C, Aubin C-E (2009) Finite element investigation of the loading rate effect on the spinal load-sharing changes under impact conditions. J Biomech 42:1252–1262

24. Wagnac E, Arnoux P-J, Garo A, Aubin C-E (2012) Finite element analysis of the influence of loading rate on a model of the full lumbar spine under dynamic loading conditions. Med Biol Eng Comput 50:903–915

25. Ogden RW (1984) Non-linear elastic deformations. Elsevier, Amsterdam

26. Wagnac E, Arnoux P-J, Garo A, El-Rich M, Aubin C-E (2011) Calibration of hyperelastic material properties of the human lumbar intervertebral disc under fast dynamic compressive loads. J Biomech Eng 133:101007

27. Garo A, Arnoux PJ, Wagnac E, Aubin CE (2011) Calibration of the mechanical properties in a finite element model of a lumbar vertebra under dynamic compression up to failure. Med Biol Eng Comput 49:1371–1379

28. Pintar FA, Yoganandan N, Myers T, Elhagediab A, Sances A (1992) Biomechanical properties of human lumbar spine ligaments. J Biomech 25:1351–1356

29. White AA, Panjabi MM (1990) Clinical biomechanics of the spine, vol 2. Lippincott, Philadelphia

30. Ivancic PC, Coe MP, Ndu AB, Tominaga Y, Carlson EJ, Rubin W, Dipl-Ing FH, Panjabi MM (2007) Dynamic mechanical properties of intact human cervical spine ligaments. Spine J 7:659–665

31. Iwaskiw AS, Armiger RS, Ott KA, Wickwire ACM, Merkle AC (2012) Response of individual thoracolumbar spine ligaments under high-rate deformation. Biomed Sci Instrum 48:194–201

32. Butt AM, Gill C, Demerdash A, Watanabe K, Loukas M, Rozzelle CJ, Tubbs RS (2015) A comprehensive review of the sub-axial ligaments of the vertebral column: part I anatomy and function. Childs Nerv Syst 31:1037–1059

33. Lasswell TL, Cronin DS, Medley JB, Rasoulinejad P (2017) Incorporating ligament laxity in a finite element model for the upper cervical spine. Spine J 17:1755–1764

34. Schmidt H, Heuer F, Drumm J, Klezl Z, Claes L, Wilke H-J (2007) Application of a calibration method provides more realistic results for a finite element model of a lumbar spinal segment. Clin Biomech 22:377–384

35. Jaramillo HE, Puttlitz CM, McGilvray K, García JJ (2016) Characterization of the L4–L5–S1 motion segment using the step-wise reduction method. J Biomech 49:1248–1254

36. Schwab F, Lafage V, Boyce R, Skalli W, Farcy J-P (2006) Gravity line analysis in adult volunteers: age-related correlation with spinal parameters, pelvic parameters, and foot position. Spine 31:E959–E967

37. Belwadi A, Yang K (2008) Response of the cadaveric lumbar spine to flexion with and without anterior shear displacement. In: Proc IRCOBI Conf, pp 397–410

38. Stemper BD, Pintar FA, Baisden JL (2015) Lumbar spine injury biomechanics. In: Accidental Injury (ed) Springer, pp 451–470

39. Tsou PM, Wang J, Khoo L, Shamie AN, Holly L (2006) A thoracic and lumbar spine injury severity classification based on neurologic function grade, spinal canal deformity, and spinal biomechanical stability. Spine J 6:636–647

40. Mitchell R, Bambach M, Toson B (2015) Injury risk for matched front and rear seat car passengers by injury severity and crash type: an exploratory study. Accid Anal Prev 82:171–179

41. Müller CW, Otte D, Decker S, Stübig T, Panzica M, Krettek C, Brand S (2014) Vertebral fractures in motor vehicle accidents–a medical and technical analysis of 33,015 injured front-seat occupants. Accid Anal Prev 66:15–19

42. Schmidt H, Galbusera F, Rohlmann A, Shirazi-Adl A (2013) What have we learned from finite element model studies of lumbar intervertebral discs in the past four decades? J Biomech 46:2342–2355

43. Siegmund GP, Chimich v, Elkin BS (2015) Role of muscles in accidental injury. In: Accidental injury (ed) Springer, pp 611–642

Éric Wagnac is an associate professor at École de technologie supérieure (Montréal) and researcher at Sacré-cœur Hospital research center. His research focuses on spinal and head pathomechanisms in traumatic conditions.

Manon Sterba is a joint-PhD candidate at Polytechnique Montréal and Aix-Marseille University. She works on the lumbar spine injury biomechanics under the supervision of Pr. Carl-Éric Aubin and Dr. Pierre-Jean Arnoux.

Léo Fradet obtained his PhD from a joint program at École de technologie supérieure (Montréal) and Aix-Marseille University on the trauma of the spine and the spinal cord.

Carl-Éric Aubin is a full professor at Polytechnique Montréal, researcher at Sainte-Justine University Hospital Center, and Canada Research Chair in Orthopedic Engineering and NSERC/Medtronic Industrial Research Chair in Spine Biomechanics.

Pierre-Jean Arnoux is a senior researcher at IFSTTAR/Aix-Marseille University and head of the Applied Biomechanics Lab. He works on human biomechanics with a special focus on the spine and sport and car accidents simulation.